

Universidade de São Paulo
Instituto de Astronomia, Geofísica e Ciências Atmosféricas
Departamento de Geofísica

Lucas Alexandre Schirbel

Reservoir Induced Seismicity at the Laúca Dam in Northwestern
Angola – Focal Mechanisms and Stress Field Estimation

São Paulo
2023

Lucas Alexandre Schirbel

Reservoir Induced Seismicity at the Laúca Dam in Northwestern Angola – Focal Mechanisms and Stress Field Estimation

Dissertação apresentada ao Departamento de
Geofísica do Instituto de Astronomia,
Geofísica e Ciências Atmosféricas da
Universidade de São Paulo como requisito
parcial para a obtenção do título de Mestre
em Ciências

Área de Concentração: Geofísica

Orientador: Prof. Dr. Marcelo Sousa de Assumpção

São Paulo

2023

Agradecimentos

À minha família por todo o apoio ao longo dos anos, minhas queridas mãe e avó Heloísa e Maria Aparecida e meu querido irmão Matheus;

Ao meu orientador Prof. Dr. Marcelo Sousa de Assumpção pelas dúvidas esclarecidas e ensinamentos ao longo de todo o desenvolvimento do projeto;

Aos professores do Departamento de Geofísica do IAG/USP Prof. Dr. Carlos Alberto Moreno Chávez e Prof. Dr. Marcelo Belentani de Bianchi pelas incontáveis ajudas ao longo dos anos com todo tipo de dúvida;

Aos colegas de mestrado e de trabalho que estiveram comigo ao longo desta jornada;

Ao IPT pela possibilidade de desenvolver este projeto de mestrado em paralelo ao meu trabalho;

À Universidade de São Paulo por oferecer ensino gratuito e de qualidade à toda população brasileira.

À PRODEL-EP e Francisco António Pereira Neto por disponibilizarem os dados que tornaram este trabalho possível.

RESUMO

A Sismicidade Induzida por Reservatórios (SIR) é um fenômeno bem documentado, com mais de 100 casos relatados em todo o mundo. O represamento de reservatórios de água altera o campo de tensão local e serve como catalisador/disparador para a liberação de tensão acumulada tectonicamente. Casos de SIR que ocorrem em regiões intraplacas são particularmente interessantes, pois proporcionam uma oportunidade de estudar o campo de tensão local e regional em áreas onde as ocorrências de terremotos são raras e essas chances são pouco comuns.

Relatamos um novo caso de SIR no sudoeste da África, na bacia do Kwanza, província de Malanje em Angola, localizada no Escudo Angolano. O reservatório de Lauca, onde ocorre a sismicidade, está situado em uma região composta principalmente de rochas graníticas e gnaissicas cobertas por uma fina camada de rochas sedimentares, e a sismicidade lá foi observada logo após o nível da água subir para cerca de 86m após o represamento inicial. A altura máxima da barragem é de 156m e o volume do reservatório é de 5,044.85 Hm³. Mais de 270 eventos foram detectados entre março/2018 e novembro/2020, e a sismicidade não cessou, indicando tanto atividade sísmica inicial quanto prolongada. A frequência de eventos com magnitude superior a 2,5 ML aumentou ao longo do tempo. O maior evento até agora teve magnitude de 3,0 ML e foi sentido em aldeias e cidades próximas.

As fases P e S para todos os eventos foram lidas manualmente, e um diagrama composto de Wadati produziu uma razão V_p/V_s de 1,710 +- 0,003 para a área do lago, compatível com a geologia local. Utilizamos a minimização de resíduos de tempo de viagem com HYPO71 e HYPOCENTER para determinar o melhor modelo de velocidade de meio espaço para a área do reservatório, que determinamos ser $V_p = 6,1$ km/s. Os ângulos de back azimuth para todos os eventos também foram determinados manualmente e usados para melhorar as localizações. As localizações epicentrais mostram que a maioria dos eventos se agrupa ao longo de duas falhas aproximadamente orientadas no sentido norte-sul, um padrão incomum em casos de SIR, mas

que pode auxiliar a determinar os mecanismos focais. Determinamos mecanismos focais para quatro dos maiores eventos na área usando a polaridade de chegada P e SH e as razões de amplitude P/S, e os comparamos com modelos do campo de tensão regional. Descobrimos que o regime de falhas na área é transpressivo e que o SH_{Max} aponta na direção SW-NE, em desacordo com os modelos geodinâmicos atuais para a placa Africana.

ABSTRACT

Reservoir Triggered Seismicity (RTS) is a well documented phenomenon, with over 100 cases reported worldwide. The impounding of water reservoirs changes the local stress field and serves as a catalyst/trigger for the release of tectonically accumulated stress. RTS cases occurring in intraplate regions are particularly interesting, since they provide an opportunity to study the local and regional stress field in areas where earthquake occurrences are rare and these chances seldom come by.

We report a new case of RTS in southwestern Africa, in the Kwanza basin, Malanje province of Angola, located in the Angolan Shield. The Lauca reservoir, where seismicity is taking place, sits atop a region composed mainly of granitic and gneissic rocks covered by a thin layer of sedimentary rocks, and seismicity there was observed shortly after the water level rose to about 90m following initial impoundment. The maximum dam height is 156m and the reservoir volume is 5,044.85 Hm³. Over 270 events were detected between March/2018 and and November/2020, and seismicity has not ceased, indicating both initial and protracted seismic activity at play. The frequency of events with magnitude larger than 2.5 ML has increased over time. The largest event so far had magnitude 3.0 ML, and was felt in nearby villages and towns.

P and S phases for all events were manually picked, and a composite Wadati diagram yielded a V_p/V_s ratio of 1.710 \pm 0.003 for the lake area, compatible with the local geology. We use minimization of travel time residuals with both HYPO71 and HYPOCENTER to determine the best half-space velocity model for the reservoir area, which we determine to be $V_p= 6.1$ km/s. Back Azimuth angles for all events were also manually determined and used to better constrain locations. Epicentral locations show that most events cluster along two roughly N-S oriented faults, an uncommon pattern in cases of RTS, but which can nonetheless aid the determination of the focal mechanisms. We determine focal mechanisms for four of the largest events in the area using both P and SH arrival polarity and P/S amplitude ratios, and compare it to models of the

regional stress field. We find that the faulting regime in the area is transpressive and that SH_{Max} points in the SW-NE direction, in disagreement with current geodynamical models of the Nubian plate.

SUMÁRIO

| | |
|---|----|
| INTRODUCTION | 11 |
| RESEARCH PAPER | 15 |
| 1 . <i>Introduction</i> | 17 |
| 2 . <i>Velocity Model and Epicenters</i> | 18 |
| 2.1 <i>Vp/Vs ratio and Vp determination</i> | 18 |
| 2.2 <i>Epicentral distribution and Waveform Cross Correlation</i> | 19 |
| 3 . <i>Focal Mechanisms Using S/P Amplitude Ratios</i> | 20 |
| 4 . <i>Local Stress Field and Model Comparison</i> | 21 |
| 5 . <i>Conclusions</i> | 22 |
| 6 . <i>Acknowledgments</i> | 23 |
| 7 . <i>References</i> | 23 |
| <i>Figures</i> | 27 |
| <i>Tables</i> | 35 |
| CONCLUSION..... | 38 |
| REFERENCES..... | 39 |

INTRODUCTION

Reservoir Triggered Seismicity (RTS) is the phenomenon where the construction and filling of water reservoirs gives rise to seismic activity in the vicinity of said enterprises. It was first associated with the filling of lake Mead in the mid 1930s (Carder 1945), and has since been observed in several locations around the world, including Brazil (Simpson 1986, Barros et al. 2018). Lake impoundment changes both elastic and pore pressure conditions in the surrounding rocks, and although these pressure changes are small compared to the tectonic loading in the crust, they may serve as a trigger to release accumulated stress. McGarr and Simpson (1997) propose a differentiation between induced earthquakes, where anthropic action is responsible for most of the stress changes or energy release in the form of earthquakes, and triggered seismicity, where human activity is merely the trigger that sets off events where most stress changes or energy accumulation in the crust happened through tectonic loading.

If we adopt this convention, Gupta (2002) then proposes that all cases involving water reservoirs can be classified under the triggered category, since the stress changes due to both elastic loading and pore pressure changes are in the order of 1 MPa, much lower than the stress drops associated with earthquakes (collectively speaking). Nevertheless, the terms “Induced” and “Triggered” earthquakes are commonly used interchangeably, that is, events which are directly related and brought about by human activities.

Triggered earthquakes usually happen in the vicinity of the engineering activities which trigger them, which means that economic and social impacts have to be taken into account when implementing these projects, since even relatively small earthquakes can have significant impact on local structures (Simpson 1986). The largest triggered earthquake recorded to date happened in the Koyna reservoir in India in 1967 causing 200 deaths, 1500 injuries and also severe damage to nearby structures (Gupta & Rastogi 1976).

Other examples of significant triggered seismicity which have caused damage to structures and nearby populations can be found in China, Greece, and the United States. The potential impacts of triggered seismicity have led to renewed efforts in monitoring water reservoirs and further studies of the physical mechanisms which give rise to them, sparking interest from the scientific community and civil society. Major projects around the world have been halted due to fears of significant damage to structures and/or nearby towns/populations. Thus the study of this phenomenon is well justified from a scientific as well as an economic and social point of view.

RTS was first reported in Brazil in the early seventies in the Carmo do Cajuru reservoir, located in the countries' southeast region. Overall, 26 cases have been reported as of 2008, with the largest magnitude of 4.2 mB and VI–VII MMI intensity observed at the Porto-Colômbia reservoir in South-Eastern Brazil. A compilation of studies carried out at several sites in Brazil by Barros et al. (2018) indicates that there is no clear correlation between local geology and earthquake triggering in the country, although igneous rocks seem to be slightly more prone to RTS than either sedimentary or metamorphic rocks. Dam tallness seems to be positively correlated to whether or not seismicity will be triggered, with dams taller than 100m showing 65% probability, however, magnitude is not, with relatively large earthquakes having been triggered by dams with a water depth of less than 50 m, where the chances of earthquakes being triggered at all is estimated to be around 2%. This lack of relationship between dam tallness and magnitude seems to hold worldwide.

Reservoir-induced seismicity can be both initial or delayed (Simpson et al. 1988). Initial seismicity is associated with the increase of shear stress due to elastic loading of the reservoir, and happens immediately after impounding, usually resulting in earthquakes of small magnitude presenting swarm-like behavior, confined to the immediate reservoir area. Delayed seismicity, on the other hand, is related to changes in pore pressure due to pressure diffusion, and is associated with larger earthquakes which can happen at significant distances from the reservoir. Both types can happen at any reservoir.

Our goal in this project is to study the seismicity triggered by the construction and subsequent impoundment of the Lauca hydroelectric reservoir in the Middle Kwanza region in Angola. Both reservoirs (Capanda and Laúca) are located near the Kwanza horst in northwestern Angola. This region is known to have been seismically active in the recent past, with a magnitude 6.0 Mw earthquake occurring 35 km from the Laúca dam on the 24th of May 1914. A magnitude 3.9 earthquake also struck the region on the 29th of May 2009, reaching intensity IV-V on the modified Mercalli Scale.

Impoundment of the Capanda reservoir began in August 2002 and was concluded on the 15th of March 2003, with the water column reaching 89m at peak capacity. Seismicity was first observed on the 23rd of June 2003, 90 days after the reservoir had reached peak storage capacity, then again on the 16th of november 2015. Both events were recorded by seismic networks operating in the vicinity of the reservoirs. A third event was registered on the 23rd of July 2013, 12 km away from the Capanda dam, reaching magnitude 2.5.

Recurring seismicity has been observed near the Laúca reservoir after impoundment in 2017, beginning on March 1st 2018, when the water column at the reservoir sat at 86m tall, and total water volume at $1.9847E+12$ m³, with these values varying slightly according to hydrological conditions. In total, more than 270 earthquakes were registered over the course of 3 years of

monitoring. This presents us with a great opportunity to study focal mechanisms and the local stress field, given the outstanding quality of the seismic records.

The results of the work conducted over the last two years were written in the form of a research paper and submitted to the journal *Tectonophysics* for publishing. They are presented in Chapter 2 of this dissertation.

RESEARCH PAPER

This chapter presents the research paper which was submitted to the journal *Tectonophysics* on 12/03/2023.

Laúca Dam: The First Reported Case of Reservoir-Induced Seismicity in the Congo Craton. Focal Mechanism Determinations and Stress Field Estimation.

Lucas Schirbel^{1,2}, Marcelo Assumpção¹, Francisco António Pereira Neto³, George Sand França⁴

¹ Universidade de São Paulo, Departamento de Geofísica do IAG/USP, Rua do Matão 1226, Cidade Universitária, 05508-900 São Paulo, SP, Brazil.

² IPT - Instituto de Pesquisas Tecnológicas do Estado de SP. Av. Prof. Almeida Prado 532 Cidade Universitária - Butantã. 05508-901 São Paulo, SP, Brazil.

³ PRODEL – Empresa Pública de Produção de Electricidade - Luanda, Município de Belas, Gaveto - Angola.

⁴ Universidade de Brasília, Observatório Sismológico, Prédio SG -13 - Campus Universitário Darcy Ribeiro - Asa Norte, SGAN - Brasília, DF.

Corresponding Author: Lucas Schirbel. e-mail: lucas.schirbel@usp.br; lschirbel@ipt.br

Abstract: We present the first case of reservoir induced seismicity (RIS) ever reported in the Congo Craton, the Laúca reservoir. Impoundment of the reservoir began in late 2017 and seismicity started in March 2018 shortly after the water level reached 86 m. Earthquakes continued to be recorded in the following years, with over 270 events detected between March/2018 and November/2020. The largest event had magnitude 3.0 ML. The dam is 156 m tall, and the total reservoir volume is 5,044.85 Hm³. The reservoir area is monitored by two stations, LAUC and ZERO. Seismic data is of high quality, with sharp P and S wave arrivals at both stations. We derive a half-space velocity model for the lake area using a composite Wadati diagram and minimization of travel time residuals, and locate 90 events with arrivals at both stations. We use S/P amplitude ratios and P and SH polarities to determine focal mechanisms for four of the largest events using FOCMEC, and estimate the local stress field from the direction of the P axes of these mechanisms. We find the faulting regime in the area to be transpressive and SH_{Max} to be in the SW-NE direction, in disagreement with current theoretical models, which predict E-W extensional tectonics and N-S oriented SH_{Max}. Our results contribute to the stress field mapping in the area which should be taken into account in future geodynamic models of the Nubian plate.

Keywords: African; Angola; Stress Field; Focal Mechanisms; Reservoir-Induced Seismicity; Nubian Plate.

1. Introduction

Reservoir Induced Seismicity (RIS) is a well-documented phenomenon, with over 100 cases reported worldwide (Wilson *et al.*, 2017). The impounding of water reservoirs significantly changes the normal and shear stresses on pre-existing fault planes through both tectonic loading and pore pressure changes and serves as a catalyst/trigger for the release of tectonically accumulated stress (Simpson, 1986; Talwani, 1997). There have been dozens of cases of RIS reported in stable continental regions (e.g., Assumpção *et al.*, 2002; Barros *et al.*, 2018; Gupta *et al.*, 1969; Sayão *et al.*, 2020). Intraplate seismicity accounts for only 5% of earth's total seismic moment release and seismicity in stable continental regions accounts for even less, around 0.5% (Sandiford and Egholm, 2008). Knowledge of the stress field in intraplate regions is of great importance in understanding plate driving forces and upper mantle dynamics (e.g., Assumpção *et al.*, 2016; Naliboff *et al.*, 2012). Thus RIS cases in intraplate environments are of great interest to seismologists seeking to understand tectonic processes, as they present an opportunity to probe the local stress field in areas where earthquake occurrences are relatively rare.

Here we present a new case of RIS, the Laúca reservoir, located in the Malanje province of Angola. It is the first case of RIS ever reported in the Congo Craton, a stable continental region. The reservoir is located in the Angolan Shield, a subdivision of the larger Craton, where stress data is scarce due to lack of monitoring in the instrumental era and low overall seismicity. The dam is 156 m tall, and the total reservoir volume is 5,044.85 Hm³. The lake started filling in November 2017, and seismicity began when the water level reached approximately 86 m in March 2018 (Figure 1). Since then over 270 events have been recorded, with the largest one having magnitude 3.0 ML. This event was felt in nearby villages and towns. The lake area is monitored by two broadband stations, LAUC and ZERO.

Station ZERO has been in operation since 2013 in the Capanda dam network, which is located upstream from Laúca reservoir. Impoundment of the older Capanda reservoir in 2002 showed no

discernible change in the natural rate of seismicity in the region. Natural earthquakes are known to have occurred in the past around the area where the reservoir is located, with a significant event of magnitude 6.0 Ms occurring 35 km from the dam in 1914 (Neto *et al.* 2018). Only one event which could possibly be associated with the operation of the Capanda reservoir was detected in the entire period since it has been in operation, a magnitude 2.2 ML earthquake in July 2013. No significant induced seismicity had been detected in the region by the Capanda network prior to the filling of Laúca dam.

Our goal in this paper is to characterize the induced seismicity taking place at Laúca reservoir and to determine focal mechanisms for the largest events in the area, thus obtaining an estimate of the local stress field. We then compare these results with the theoretical models currently in place for the state of lithospheric stress in the Nubian plate.

2. Velocity Model and Epicenters

2.1 V_p/V_s ratio and V_p determination

P and S arrivals for all events recorded at both stations (90 in total) were manually picked to ensure accuracy. Arrivals are impulsive and sharp (Figure 2), which allows precise picking. A V_p/V_s ratio of 1.710 ± 0.003 (Figure 3) was determined using a composite Wadati Diagram (Kisslinger & Engdahl, 1973). This ratio is typical of felsic rocks, and compatible with the local geology, which is composed mostly of granitic and gneissic rocks (clay schists and coarse-grained granites) covered by a thin sedimentary layer.

We derive a half-space velocity model for the lake area by fixing the V_p/V_s ratio at 1.710 and minimizing travel time residuals. We start by using the program HYPOCENTER (Lienert *et al.*, 1986) to obtain an estimate of the initial location for each event using back azimuths, which were manually measured from particle motion plots for all events. An error of 10° was allowed for all back azimuths, to account for possible uncertainties in station orientation and in the measurements. The epicenters obtained from this procedure were then inserted into HYPO71 (Lee & Jahr, 1972) as new starting

locations for each event, in order to relocate the hypocenters more precisely. HYPO71 was chosen to test different depths and to refine locations since it yields a smaller total rms residual in the final solutions when compared to HYPOCENTER. We construct a single layer ranging from 0 km to 5 km with uniform velocity and test V_p values between 5.5 km/s and 6.5 km/s, the expected range of crustal V_p velocities in shields (Christensen & Mooney, 1995).

Depth is not well constrained and was fixed at 2 km, which is the median value obtained when letting it vary. With depth fixed the best velocity model yields $V_p = 6.1$ km/s with $RMS = 0.007$ s. The final epicentral locations are shown in Figure 4.

2.2 Epicentral distribution and Waveform Cross Correlation

The epicentral distribution seen at Laúca is uncommon in cases of RIS where events tend to be spread in large volumes. Events in Laúca cluster along two main faults roughly N-S oriented, one located to the north of the lake and another one to the southeast. This observed pattern could be due to fault reactivation in the vicinity of the reservoir. Earthquakes in the northernmost fault (from here onward referred to as the main fault) migrate outwards over time, as shown in Figure 4, a pattern which is consistent with models of pore pressure diffusion and epicentral migration proposed for RIS (e.g., Talwani, 1997). This consistency with established physical models suggests that events are well located with respect to one another in the N-S direction by employing the back azimuths. In the southeast fault (the secondary fault) all events happen in the span of a few weeks and no discernible migration pattern can be seen.

We carry out waveform cross-correlation to improve relative pick times for P and S arrivals and ascertain that the epicentral distribution observed is not simply an artifact arising from a lack of azimuthal coverage. We choose eight of the largest events, with magnitudes ranging from 1.8 ML to 3.0 ML, listed in Table 1, five on the main fault and three on the secondary fault, to be correlated with one another at each station. We use the code developed by Ciardelli & Assumpção (2019) for the CC analysis. An example of the program's output is shown in Figure 5. Parameters for the cross-correlation were chosen based on visual inspection of P and S pulses on the seismograms. Since most

events are small, a 0.4 second window extending after the phase arrival time and a 0.1 second window before arrival time works well enough for both P and S arrivals. A BW filter of 1.5 to 15 Hz was applied to all seismograms, in accordance with the criteria adopted in Schaff & Waldhauser (2005), so as to reduce long-period instrument noise and less similar high frequencies. The maximum allowed lag was 0.1 seconds for both P and S phases at both stations. We choose event 2 as the master/reference event, since its magnitude is intermediate with relation to the others, and we select a cut off value of 0.5 for the cross-correlation, i.e., all phases with a cross-correlation coefficient of 0.5 or greater have their pick times improved. The results are listed in Table 2.

Although cross-correlation values are high for both phases in most events, no significant change in epicentral location is found after relocation with the improved pick times for any of the events (Figure 6). We thus conclude that while epicentral uncertainties might be large, our events are well located with respect to one another and delineate two faults in the reservoir area, oriented in the NNE – SSW direction. We are able to constrain events to the north and south of the station line using back azimuths, and small changes in arrival times do not significantly change either relative location in the N-S direction or undo the observed fault pattern. This information is useful when attempting to identify fault and auxiliary planes in the focal mechanism solutions.

3. Focal Mechanisms Using S/P Amplitude Ratios

Amplitude ratios are useful in constraining focal mechanisms (Kisslinger, 1980; Kisslinger *et al.*, 1982; Wu *et al.*, 2015), especially where data is scarce and P and S first motions alone are not enough to obtain a solution. We use the program FOCMEC (Snoke, 1984; Snoke *et al.*, 2003) to determine focal mechanisms for all events listed in Table 1. Events were chosen based on their magnitude, as visual inspection shows they are at the lower limit of the S/N ratio where it is possible to measure the SV arrivals on the vertical component, and also location, to test whether earthquakes located on different faults had similar mechanisms. We search the entire focal sphere (dip, strike, slip) in steps of 5° for all parameters, with the exception of event number 1, where we used steps of 10°. Both P and SH polarities and SH/P, SV/SH and SV/P displacement amplitude ratios were used to constrain the nodal planes (Table 3). SV amplitudes were measured on the vertical component, since they are less disturbed

by low-velocity zones near the surface (Booth & Crampin, 1985). Arrivals are very clear so we allow no polarity errors, and we set a maximum allowed error of $\log_{10}(A) = 0.3$ for the measured amplitude ratios to account for possible contamination by SP arrivals and near-surface effects. We obtain the emergence angles from the P-wave particle motions, and assume the S-wave emergence angles to be the same as for the P-waves. All amplitudes were corrected for the free-surface effect. Events are close to both stations (15 ~ 30 km) so no anelastic attenuation corrections were needed.

We find that for events 2, 3 and 7 at least one of the stations is located too close to one of the nodal planes, which makes it hard to get a reliable estimate of the emergence angles and amplitude ratios. We are unable to measure the SV amplitudes for event 8, and since we are working with only two stations, we only use events where the three amplitude ratios can be reliably obtained. We are able to determine focal mechanisms for four of the events, numbers 1, 4, and 5 on the main fault, and event 6 on the secondary fault (Figure 7). Mechanisms are generally well constrained, with small variations observed between different solutions. Three of the mechanisms are right-lateral strike-slip (1, 5 and 6) and one is an oblique reverse fault (event 4).

Event 5 is an aftershock of event 1 and happened on the same day a few hours later. They are located close to one another, and the best solutions for each one are almost identical, yielding a right-lateral strike-slip fault plane in the N-S direction, in agreement with the observed epicentral distribution. Event 1 shows slightly more spread in the possible dip of the N-S striking fault than event 5, but P-axis direction does not vary significantly between the acceptable solutions. The best solutions for events 1 and 5 have an rms residual of the log(amplitude ratio) of 0.05 and 0.13, respectively, and a maximum absolute residual for any given amplitude ratio of 0.10 for event 1 and 0.19 for event 5. Event number 6, located on the secondary fault, also displays the same pattern of right-lateral strike slip faulting, with the P-wave polarities switched when compared with events 1 and 5. The rms residual for the event is 0.13 with a total maximum absolute residual of 0.21. Event number 4 is the only one whose focal mechanism is significantly different from the others, displaying a reverse fault with an rms residual of 0.09 and a maximum absolute residual of 0.14.

4. Local Stress Field and Model Comparison

A schematic of the possible fault motions in the area as inferred from the epicentral distribution and focal mechanisms is presented in [Figure 8](#). Event numbers 1 and 5 suggest a strike-slip fault at the northern edge of the reservoir with right-lateral motion. Event 6, the only one whose mechanism could be determined on the secondary fault, is also right-lateral strike-slip, and suggests a single fault striking SSW-NNE in that area of the reservoir. Regarding event 4, its location relative to events 1 and 5 suggests that although the observed epicentral migration seems to take place along a single fault, in reality we have at least two different faults being reactivated at the northern edge of the reservoir. In the region where event 4 is located we see slightly more spread in the epicenters when compared to the region where events 1 and 5 are located, which is compatible with a reverse mechanism.

The seismic distribution in the lake area coupled with the focal mechanisms indicates that the faulting regime at Laúca reservoir is transpressive. The right-lateral motion of the strike-slip faults located on opposite sides of the reservoir create a compressive region in the middle of the lake, where we see thrust faulting. P axes from all four focal mechanisms consistently point in the SW-NE direction, albeit with slightly different angles. Even though the direction of maximum compressive stress (S_1) can differ significantly from the P axis ([McKenzie, 1969](#)), being anywhere in the dilatational quadrant, the P axis direction is still a good first order approximation to the local stress field for strike slip and reverse mechanisms, since the most probable direction for S_1 is approximately 30° from the fault plane (e.g. [Zoback, 1992](#)). Thus we can say that SH_{max} in the lake area points roughly in the SW-NE direction, in disagreement with current geodynamic models (e.g. [Coblentz & Sandiford, 1994](#); [Stamps *et al.*, 2014](#); [Mahatsente & Coblentz, 2015](#)) which predict extensional or transextensional tectonics in this region with SH_{max} pointing in the N-S direction. This disagreement between the models and observations most likely arises from the lack of stress data in the region up until now.

5. Conclusions

Geodynamical models need to take into account the local stress field of the interior of continents if they hope to explain plate motion and tectonic evolution. Stable continental regions are areas with very low seismicity and as such well-recorded events for which focal mechanisms can be obtained are a rare

find. In this respect, induced seismicity, when recorded by a local network, such as in Laúca, presents a great opportunity to study regional tectonics and the local stress field. Local events at Laúca dam are generally small (magnitudes ≤ 3.0 ML), but very clearly recorded, and S/P amplitude ratios alongside P and SH polarities can be used to better determine the focal mechanisms.

We characterize the seismicity induced by the reservoir and obtain reasonably well constrained focal mechanisms, which suggest that the faulting regime in the region is transpressive, in disagreement with previous studies indicating extensional tectonics in the area. A rough estimate of the local stress field from the P axes of the mechanisms indicates that SH_{Max} points in the SW-NE direction, similar to what is seen further to the East in the models of [Stamps *et al.* \(2014\)](#) and [Mahatsente & Coblentz \(2015\)](#). Our study provides a new constraint for future geodynamic modeling of the stress field in the Nubian plate, and adds a new case of RIS to the worldwide database.

Acknowledgments

We thank PRODEL-EP and Capanda Hydroelectric Company for allowing publication of the Laúca case, and IPT for the allotted hours to carry out this work. GSF thanks CNPq PQ grants.

The Capanda Dam Monitoring Dept (PRODEL-EP) installed the stations and carried out preliminary analyses. PRODEL – EP is responsible for the operation of all hydroelectric power plants in Angola, including Laúca.

References

Assumpção, M., Marza, V., Barros, L., Chimpliganond, C., Soares, J. E., Carvalho, J., ... & Cabral, E. (2002). Reservoir-induced seismicity in Brazil. *The Mechanism of Induced Seismicity*, 597-617.

Assumpção, M., Dias, F. L., Zevallos, I., & Naliboff, J. B. (2016). Intraplate stress field in South America from earthquake focal mechanisms. *Journal of South American Earth Sciences*, 71, 278-295.

Barros, L. V., Assumpção, M., Ribotta, L. C., Ferreira, V. M., de Carvalho, J. M., Bowen, B. M., & Albuquerque, D. F. (2018). Reservoir-triggered seismicity in Brazil: Statistical characteristics in a midplate environment. *Bulletin of the Seismological Society of America*, *108*(5B), 3046-3061.

Booth, D. C., & Crampin, S. (1985). Shear-wave polarizations on a curved wavefront at an isotropic free surface. *Geophysical Journal International*, *83*(1), 31-45.

Christensen, N. I., & Mooney, W. D. (1995). Seismic velocity structure and composition of the continental crust: A global view. *Journal of Geophysical Research: Solid Earth*, *100*(B6), 9761-9788.

Ciardelli, C., & Assumpção, M. (2019). Rupture lengths of intraplate earthquakes in Brazil determined by relative location of aftershocks: evidence for depth dependence of stress drops. *Journal of South American Earth Sciences*, *89*, 246-258.

Coblentz, D. D., & Sandiford, M. (1994). Tectonic stresses in the African plate: Constraints on the ambient lithospheric stress state. *Geology*, *22*(9), 831-834.

Gupta, H., Narain, H., Rastogi, B. K., & Mohan, I. (1969). A study of the Koyna earthquake of December 10, 1967. *Bulletin of the Seismological Society of America*, *59*(3), 1149-1162.

Kisslinger, C., & Engdahl, E. R. (1973). The interpretation of the Wadati diagram with relaxed assumptions. *Bulletin of the Seismological Society of America*, *63*(5), 1723-1736.

Kisslinger, C. (1980). Evaluation of S to P amplitude ratios for determining focal mechanisms from regional network observations. *Bulletin of the Seismological Society of America*, *70*(4), 999-1014.

Kisslinger, C., Bowman, J. R., & Koch, K. (1982). Determination of focal mechanism from SV/P amplitude ratios at small distances. *Physics of the Earth and planetary interiors*, *30*(2-3), 172-176.

Lee, W. H. K., & Lahr, J. C. (1972). *HYPO71: A computer program for determining hypocenter, magnitude, and first motion pattern of local earthquakes* (p. 100). US Department of the Interior, Geological Survey, National Center for Earthquake Research.

Lienert, B. R., Berg, E., & Frazer, L. N. (1986). HYPOCENTER: An earthquake location method using centered, scaled, and adaptively damped least squares. *Bulletin of the Seismological Society of America*, 76(3), 771-783.

Mahatsente, R., & Coblenz, D. (2015). Ridge-push force and the state of stress in the Nubia-Somalia plate system. *Lithosphere*, 7(5), 503-510.

McKenzie, D. P. (1969). The relation between fault plane solutions for earthquakes and the directions of the principal stresses. *Bulletin of the Seismological Society of America*, 59(2), 591-601.

Naliboff, J. B., Lithgow-Bertelloni, C., Ruff, L. J., & de Koker, N. (2012). The effects of lithospheric thickness and density structure on Earth's stress field. *Geophysical Journal International*, 188(1), 1-17.

Neto, F. A. P., França, G. S., Condori, C., Sant'Anna Marotta, G., & Chimpliganond, C. N. (2018). Angola seismicity. *Journal of Seismology*, 22, 1113-1126.

Sandiford, M., & Egholm, D. L. (2008). Enhanced intraplate seismicity along continental margins: Some causes and consequences. *Tectonophysics*, 457(3-4), 197-208.

Sayão, E., França, G. S., Holanda, M., & Gonçalves, A. (2020). Spatial database and website for reservoir-triggered seismicity in Brazil. *Natural Hazards and Earth System Sciences*, 20(7), 2001-2019.

Schaff, D. P., & Waldhauser, F. (2005). Waveform cross-correlation-based differential travel-time measurements at the Northern California Seismic Network. *Bulletin of the Seismological Society of America*, 95(6), 2446-2461.

Simpson, D. W. (1986). Triggered earthquakes. *Annual Review of Earth and Planetary Sciences*, 14(1), 21-42.

Snoke, J. A., Lee, W. H. K., Kanamori, H., Jennings, P. C., & Kisslinger, C. (2003). FOCMEC: Focal mechanism determinations. *International handbook of earthquake and engineering seismology*, 85, 1629-1630.

Snoke, J. A. (1984). A program for focal mechanism determination by combined use of polarity and SV-P amplitude ratio data. *Earthquake notes*, 55, 15.

Stamps, D. S., Flesch, L. M., Calais, E., & Ghosh, A. (2014). Current kinematics and dynamics of Africa and the East African Rift System. *Journal of Geophysical Research: Solid Earth*, 119(6), 5161-5186.

Talwani, P. (1997). On the nature of reservoir-induced seismicity. *Pure and applied Geophysics*, 150, 473-492.

Wilson, M. P., Foulger, G. R., Gluyas, J. G., Davies, R. J., & Julian, B. R. (2017). HiQuake: The human-induced earthquake database. *Seismological Research Letters*, 88(6), 1560-1565.

Wu, Q., Chapman, M. C., & Beale, J. N. (2015). The aftershock sequence of the 2011 Mineral, Virginia, earthquake: Temporal and spatial distribution, focal mechanisms, regional stress, and the role of Coulomb stress transfer. *Bulletin of the Seismological Society of America*, 105(5), 2521-2537.

Zoback, M. L. (1992). First-and second-order patterns of stress in the lithosphere: The World Stress Map Project. *Journal of Geophysical Research: Solid Earth*, 97(B8), 11703-11728.

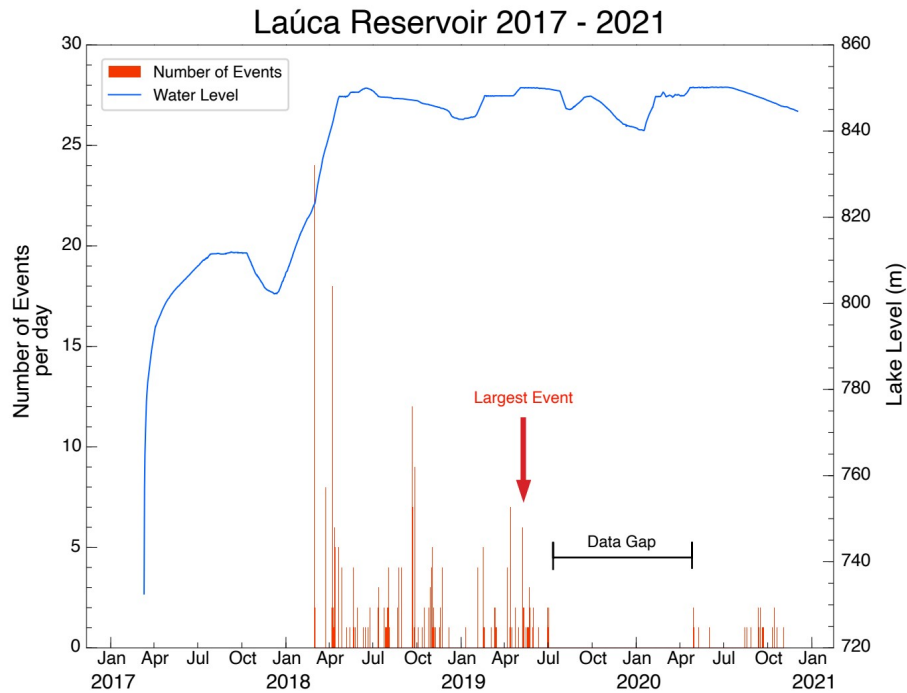


Figure 1: Event frequency (red bars) x Water level (blue line) for Laúca reservoir between Jan/2017 and Jan/2021. Seismicity started after the water level reached around 86m in march/2018, and has continued to the present day. The largest event (red arrow) occurred in May/2019 on the northern margin of the lake with magnitude 3.0 ML. All 278 events recorded in the period are shown, including earthquakes recorded at a single station.

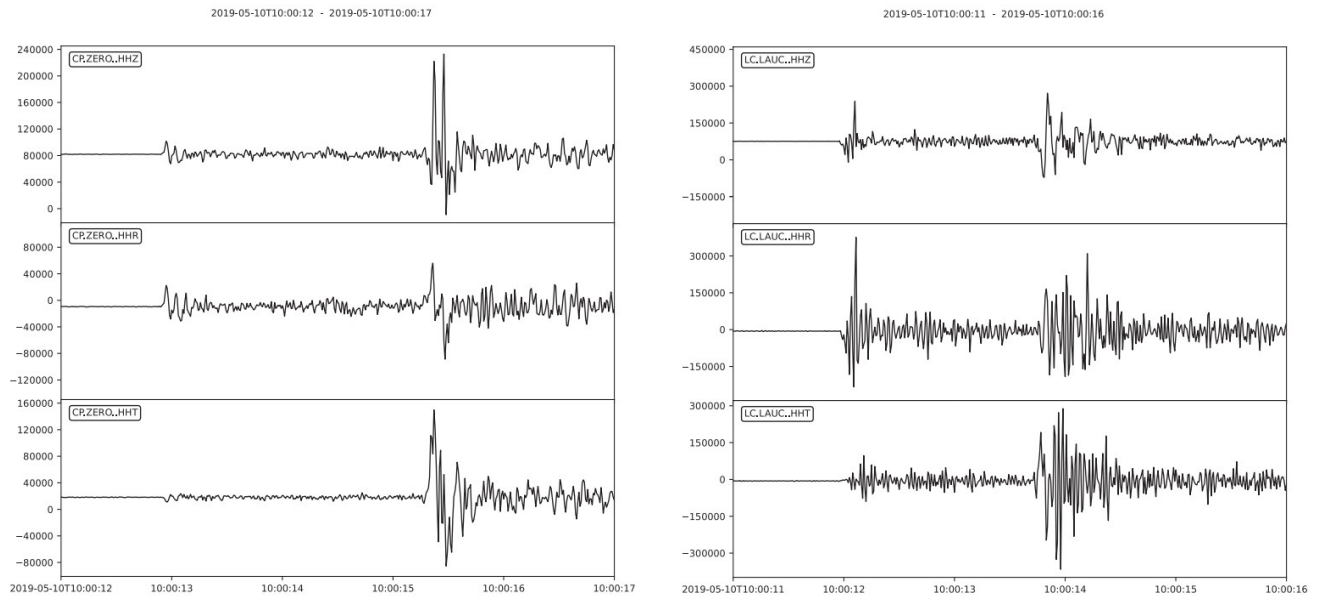


Figure 2: Unfiltered and rotated (ZRT) seismograms registered at stations ZERO (left) and LAUC (right) for the largest event recorded in the period (3.0 ML) in 2019-05-10 10:00:09 (UTC). Arrivals are impulsive and very sharp at both stations, allowing good measurements of both the P and SH polarities and amplitude ratios.

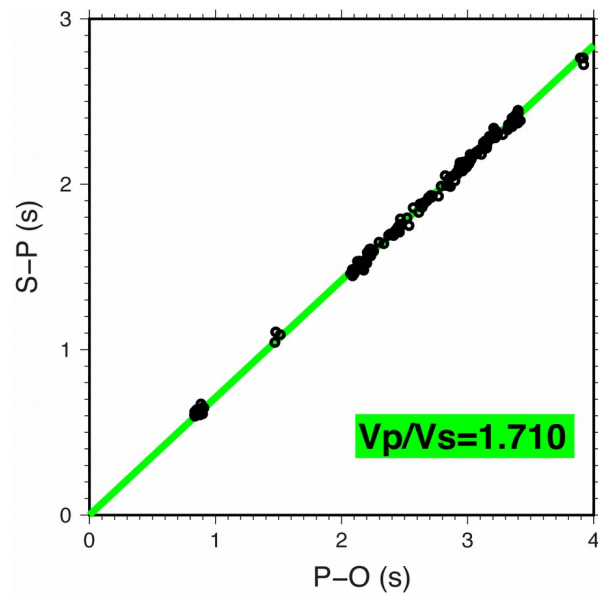


Figure 3: Composite Wadati diagram for the 90 events listed in the catalog in [Table 1](#). We find a $V_p/V_s = 1.710 \pm 0.003$, which is in agreement with the local geology. Most of the region sits atop granitic rocks covered by a thin layer of sedimentary rocks in some places.

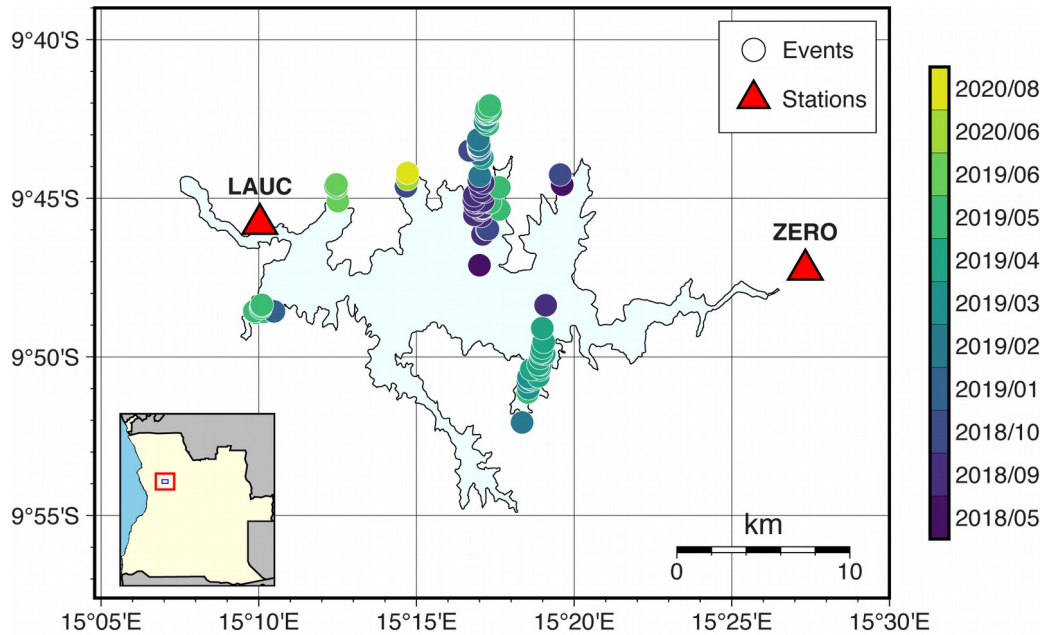


Figure 4: Final event locations (colored circles) using the best velocity model for the lake area ($V_p = 6.1$ km/s, $V_p/V_s = 1.710$). The events shown here are those recorded at both stations (LAUC and ZERO). Most events cluster along two faults roughly oriented in the N-S direction. The color bar shows the year and month in which each event occurred. We see a clear outward migration pattern over time on the main fault, located at the northern edge of the reservoir, which suggests that it is being reactivated as pore pressure diffuses. On the southern fault, events happen almost all on the same month, and no clear migration pattern is discernible.

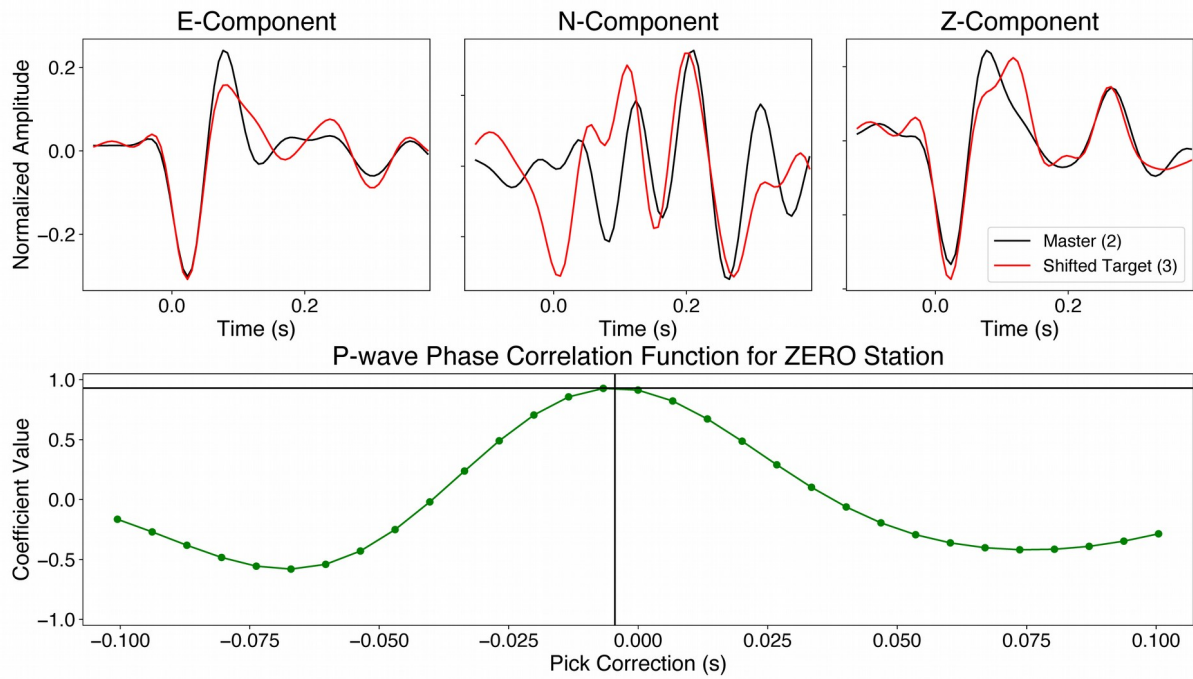


Figure 5: Top panel: Example of waveform cross-correlation at station ZERO for the P phase of events 2 (reference event, black line) and 3 (target event, red line). Bottom panel: The maximum correlation coefficient (green line) indicates the pick correction to be applied to the target event P-wave arrival time.

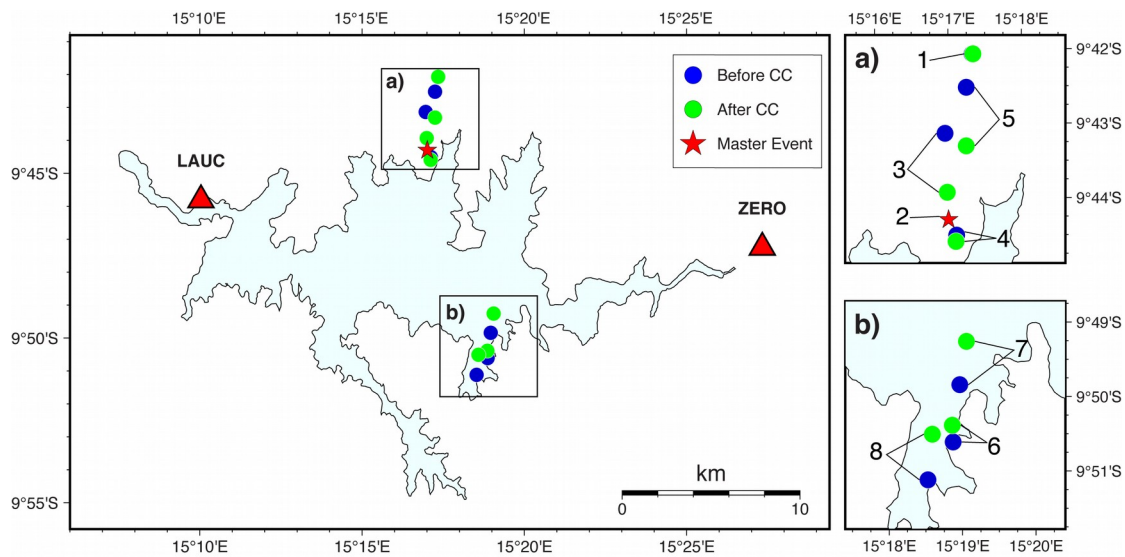


Figure 6: Event locations before cross-correlation (blue circles) and after cross correlation and pick time corrections (green circles). The reference event (red star) is located on the main fault. Panels a) and b) are zoomed in views of events on the northern and southern faults, respectively. Epicentral change for event number 1 was negligible, so green and blue circles overlap. Overall, we see a migration pattern towards the station line, but no significant changes in the E-W direction, preserving the observed fault pattern.

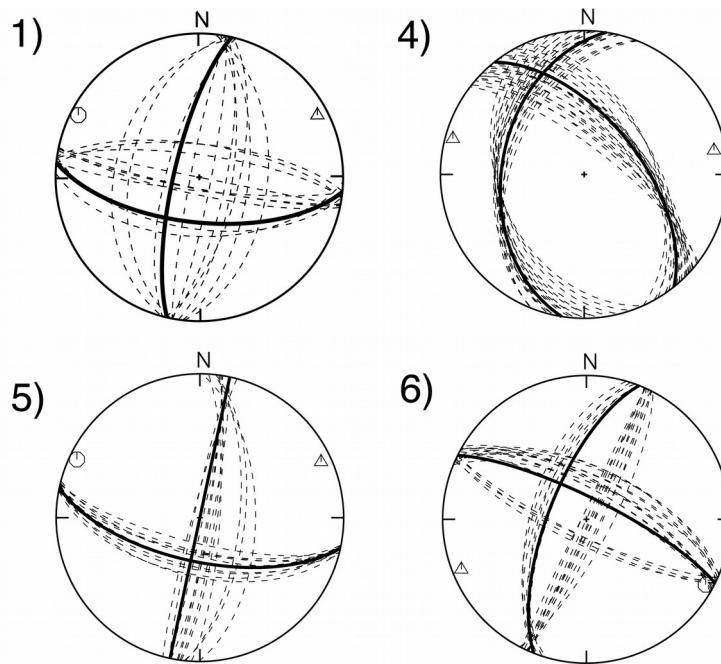


Figure 7: FOCMEC solutions for events 1, 4, 5 and 6. Dashed lines show all acceptable solutions obtained for the input amplitude ratios and solid lines show the best nodal plane solution. Triangles and circles indicate negative and positive P polarities, respectively. SV/P, SH/P and SV/SH ratios were used at both stations for all solutions. No polarity errors were allowed since arrivals are impulsive and clear. A maximum rms residual of 0.30 for the $\log(\text{amplitude ratio})$ was set to allow for near-surface effects and uncertainties. Projections are all lower hemisphere.

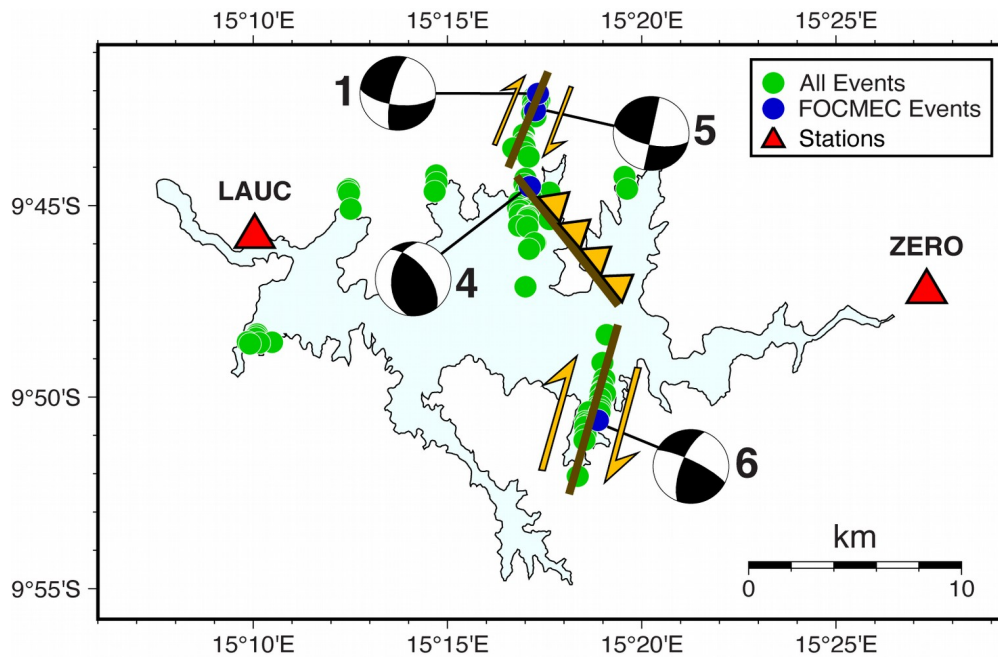


Figure 8: Seismotectonic scheme of the lake area. Brown lines show possible faults in the reservoir area based on the observed epicentral distribution and focal mechanisms, while yellow arrows indicate possible fault motion. Focal mechanisms for events on the main fault (located in the northern margin) vary in type, with events 1 and 5 exhibiting right-lateral strike-slip faulting, and event 4 displaying reverse faulting. On the secondary fault (southern margin) event number 6 is also a right-lateral strike-slip mechanism. The resulting fault orientations suggest a transpressive faulting regime in the lake area, with the offset right-lateral motion at both faults producing compression in the area in between.

Table 1: Events chosen for waveform cross-correlation and focal mechanism determination. Event number 2 was chosen as the reference/master event for the cross correlation analyses. Five events are located on the northernmost fault (main fault) and three on the southeast fault (secondary fault).

| Origin Time (UTC) | Event ID | Latitude | Longitude | Magnitude (ML) | Fault |
|---------------------|----------|----------|-----------|----------------|-----------------|
| 2019-05-10 10:00:09 | 1 | -9.7012 | 15.2888 | 3.0 | Main fault |
| 2019-02-05 05:17:30 | 2 | -9.7383 | 15.2835 | 2.5 | Main fault |
| 2019-02-16 23:21:26 | 3 | -9.7190 | 15.2827 | 2.3 | Main fault |
| 2018-09-22 18:52:23 | 4 | -9.7418 | 15.2853 | 2.1 | Main fault |
| 2019-05-10 14:54:07 | 5 | -9.7087 | 15.2875 | 2.6 | Main Fault |
| 2019-04-13 19:22:08 | 6 | -9.8435 | 15.3145 | 2.2 | Secondary fault |
| 2019-04-14 13:10:32 | 7 | -9.8307 | 15.3160 | 2.0 | Secondary fault |
| 2019-05-22 07:53:43 | 8 | -9.8520 | 15.3088 | 1.6 | Secondary fault |

Table 2: Cross-Correlation results for all events using event 2 as reference. Bold numbers indicate a cross-correlation coefficient greater than 0.5. All picks where the cross-correlation value was greater than the 0.5 threshold were improved. Event number 2 was chosen as the master/reference event, due to its location and magnitude.

| Station | Phase | Event Number | | | | | | | |
|---------|-------|--------------------------|----------|-------------|-------------|-------------|-------------|-------------|-------------|
| | | 1 | 2 | 3 | 4 | 5 | 6 | 7 | 8 |
| | | Cross-Correlation Values | | | | | | | |
| LAUC | P | 0.59 | 1 | 0.77 | 0.56 | 0.24 | 0.29 | 0.61 | 0.61 |
| | S | 0.61 | 1 | 0.84 | 0.59 | 0.61 | 0.58 | 0.66 | 0.66 |
| ZERO | P | 0.46 | 1 | 0.93 | 0.94 | 0.55 | 0.83 | 0.81 | 0.84 |
| | S | 0.59 | 1 | 0.94 | 0.61 | 0.75 | 0.18 | 0.47 | 0.77 |

Table 3: Amplitude ratios for the best nodal plane solutions for all events where focal mechanism determination was possible.

Event 1 - 2019-05-10 10:00:09 (UTC). Strike = 193, dip = 76, slip = -153

P-axis Azimuth/Plunge: 57/29, T-axis Azimuth/Plunge: 323/08

| Station | Distance (km) | Azimuth (°) | Amplitude ratio | Log(amplitude ratio) | | |
|---------|------------------|----------------|--------------------|----------------------|--------|-------|
| | | | | obs. | theor. | res. |
| LAUC | 15.0 | 242.7 | <i>SV/P</i> | 0.34 | 0.32 | 0.02 |
| | | | <i>SH/P</i> | 0.04 | 0.12 | -0.08 |
| | | | <i>SV/SH</i> | 0.30 | 0.20 | -0.10 |
| ZERO | 20.6 | 117.6 | <i>SV/P</i> | 0.22 | 0.24 | -0.02 |
| | | | <i>SH/P</i> | 0.66 | 0.70 | -0.04 |
| | | | <i>SV/SH</i> | -0.45 | -0.47 | 0.02 |

Event 4 - 2018-09-22 18:52:23 (UTC). Strike = 321, dip = 59, slip = 60

P-axis Azimuth/Plunge: 72/09, T-axis Azimuth/Plunge: 180/63

| Station | Distance (km) | Azimuth (°) | Amplitude ratio | Log(amplitude ratio) | | |
|---------|------------------|----------------|--------------------|----------------------|--------|-------|
| | | | | obs. | theor. | res. |
| LAUC | 13.2 | 259.5 | <i>SV/P</i> | -0.34 | -0.30 | -0.04 |
| | | | <i>SH/P</i> | -0.02 | -0.12 | 0.10 |
| | | | <i>SV/SH</i> | -0.32 | -0.18 | -0.14 |
| ZERO | 19.3 | 105.2 | <i>SV/P</i> | 0.07 | 0.14 | -0.07 |
| | | | <i>SH/P</i> | 0.44 | 0.53 | -0.09 |
| | | | <i>SV/SH</i> | -0.36 | -0.40 | 0.04 |

Event 5 - 2019-05-10 14:54:07 (UTC). Strike = 12, dip = 90, slip = 155.

P-axis Azimuth/Plunge: 60/17, T-axis Azimuth/Plunge: 324/17

| Station | Distance (km) | Azimuth (°) | Amplitude ratio | Log(amplitude ratio) | | |
|---------|------------------|----------------|--------------------|----------------------|--------|-------|
| | | | | obs. | theor. | res. |
| LAUC | 14.5 | 245.3 | <i>SV/P</i> | -0.11 | 0.04 | -0.15 |
| | | | <i>SH/P</i> | -0.07 | 0.07 | -0.14 |
| | | | <i>SV/SH</i> | -0.04 | -0.03 | -0.01 |
| ZERO | 20.4 | 115.3 | <i>SV/P</i> | 0.48 | 0.57 | -0.09 |
| | | | <i>SH/P</i> | 0.72 | 0.91 | -0.19 |
| | | | <i>SV/SH</i> | -0.24 | -0.34 | 0.10 |

Event 6 - 2019-04-13 19:22:08 (UTC). Strike = 202, dip = 69, slip = 167.

P-axis Azimuth/Plunge: 68/06, T-axis Azimuth/Plunge: 161/24

| Station | Distance (km) | Azimuth (°) | Amplitude ratio | Log(amplitude ratio) | | |
|---------|------------------|----------------|--------------------|----------------------|--------|-------|
| | | | | obs. | theor. | res. |
| LAUC | 18.4 | 298.7 | <i>SV/P</i> | 0.99 | 0.96 | 0.03 |
| | | | <i>SH/P</i> | 1.49 | 1.60 | -0.11 |
| | | | <i>SV/SH</i> | -0.50 | -0.64 | 0.14 |
| ZERO | 16.7 | 68.2 | <i>SV/P</i> | -0.00 | 0.14 | -0.14 |
| | | | <i>SH/P</i> | -0.48 | -0.27 | -0.21 |
| | | | <i>SV/SH</i> | 0.48 | 0.41 | 0.07 |

CONCLUSIONS

We were able to fully characterize the seismicity occurring in and around Láuca reservoir, with respect to location, magnitude, epicentral distribution, focal mechanisms and seismotectonics.

We observe a seismic pattern which is not common in cases of RTS, and which indicates faults being reactivated in the vicinity of the reservoir. We ensure that the observed pattern is not simply due to a lack of station coverage by employing all available information when locating the earthquakes, including manually measured back azimuths for all events, and the results are corroborated by the relative epicentral distribution, which follows a time-spatial pattern in agreement with physical models of pore pressure diffusion.

We manage to determine focal mechanisms using P and SH polarities and S/P amplitude ratios for 4 events well distributed around the reservoir area. The mechanisms show strike-slip and reverse faulting, and their distribution allows us to come up with a seismotectonic scheme which can explain the observed stresses. We find that the faulting regime in the area is transpressive, in disagreement with current models for the region obtained from geoid undulations, which predict a predominantly extensive tectonic regime. In addition to this, SH_{Max} is also oriented in the SW-NE direction, and is consistent among the different mechanisms, also in contradiction with current models which put it in the N-S direction. This result has important implications in future geodynamic modelling of the Nubian plate, as it shows that, contrary to what is currently believed, even at high altitudes (>500 m) compressive stresses still dominate the stress field in this region of Africa. Hence our work provides a very useful constraint in a region where stress data is very sparse.

We will continue to study the stress field in the region, and will try to calculate the stress tensor to achieve a more quantitative measure of the stress field in the reservoir area. We will also attempt to model the poro-elastic response of the reservoir to the water load during impoundment and subsequent years, and compare it to water-level variations to gain a better understanding of the pore pressure diffusion mechanism in the lake area.

References

- Assumpção, M., Marza, V., Barros, L., Chimpliganond, C., Soares, J. E., Carvalho, J., ... & Cabral, E. (2002). Reservoir-induced seismicity in Brazil. *The Mechanism of Induced Seismicity*, 597-617.
- Assumpção, M., Dias, F. L., Zevallos, I., & Naliboff, J. B. (2016). Intraplate stress field in South America from earthquake focal mechanisms. *Journal of South American Earth Sciences*, 71, 278-295.
- Barros, L. V., Assumpção, M., Ribotta, L. C., Ferreira, V. M., de Carvalho, J. M., Bowen, B. M., & Albuquerque, D. F. (2018). Reservoir-triggered seismicity in Brazil: Statistical characteristics in a midplate environment. *Bulletin of the Seismological Society of America*, 108(5B), 3046-3061.
- Booth, D. C., & Crampin, S. (1985). Shear-wave polarizations on a curved wavefront at an isotropic free surface. *Geophysical Journal International*, 83(1), 31-45.
- Carder, D.S., 1945. Seismic investigations in the Boulder Dam area, 1940 – 1944, and the influence of reservoir loading on earthquake activity. *Bull. Seismol. Soc. Am.* 35, 175 – 192.
- Christensen, N. I., & Mooney, W. D. (1995). Seismic velocity structure and composition of the continental crust: A global view. *Journal of Geophysical Research: Solid Earth*, 100(B6), 9761-9788.
- Ciardelli, C., & Assumpção, M. (2019). Rupture lengths of intraplate earthquakes in Brazil determined by relative location of aftershocks: evidence for depth dependence of stress drops. *Journal of South American Earth Sciences*, 89, 246-258.

Coblentz, D. D., & Sandiford, M. (1994). Tectonic stresses in the African plate: Constraints on the ambient lithospheric stress state. *Geology*, 22(9), 831-834.

Gupta, H.K., A review of recent studies of triggered earthquakes by artificial water reservoirs with special emphasis on earthquakes in Koyna, India, *Earth-Science Reviews*, Volume 58, Issues 3–4, 2002, Pages 279-310, ISSN 0012-8252.

Gupta, H., Narain, H., Rastogi, B. K., & Mohan, I. (1969). A study of the Koyna earthquake of December 10, 1967. *Bulletin of the Seismological Society of America*, 59(3), 1149-1162.

Gupta, H. K., Rastogi, B. K. 1976. Dams and Earthquakes. Amsterdam : Elsevier. 299 pp.

Kisslinger, C., & Engdahl, E. R. (1973). The interpretation of the Wadati diagram with relaxed assumptions. *Bulletin of the Seismological Society of America*, 63(5), 1723-1736.

Kisslinger, C. (1980). Evaluation of S to P amplitude ratios for determining focal mechanisms from regional network observations. *Bulletin of the Seismological Society of America*, 70(4), 999-1014.

Kisslinger, C., Bowman, J. R., & Koch, K. (1982). Determination of focal mechanism from SV/P amplitude ratios at small distances. *Physics of the Earth and planetary interiors*, 30(2-3), 172-176.

Lee, W. H. K., & Lahr, J. C. (1972). *HYPO71: A computer program for determining hypocenter, magnitude, and first motion pattern of local earthquakes* (p. 100). US Department of the Interior, Geological Survey, National Center for Earthquake Research.

Lienert, B. R., Berg, E., & Frazer, L. N. (1986). HYPOCENTER: An earthquake location method using centered, scaled, and adaptively damped least squares. *Bulletin of the Seismological Society of America*, 76(3), 771-783.

Mahatsente, R., & Coblenz, D. (2015). Ridge-push force and the state of stress in the Nubia-Somalia plate system. *Lithosphere*, 7(5), 503-510.

McGarr, Arthur F. and Simpson, David (1997) A broad look at induced and triggered seismicity. In: Rockburst and seismicity in mines. Balkema, Rotterdam, pp. 385-396. ISBN 90 5410 8908.

McKenzie, D. P. (1969). The relation between fault plane solutions for earthquakes and the directions of the principal stresses. *Bulletin of the Seismological Society of America*, 59(2), 591-601.

Naliboff, J. B., Lithgow-Bertelloni, C., Ruff, L. J., & de Koker, N. (2012). The effects of lithospheric thickness and density structure on Earth' s stress field. *Geophysical Journal International*, 188(1), 1-17.

Neto, F. A. P., França, G. S., Condori, C., Sant'Anna Marotta, G., & Chimpliganond, C. N. (2018). Angola seismicity. *Journal of Seismology*, 22, 1113-1126.

Sandiford, M., & Egholm, D. L. (2008). Enhanced intraplate seismicity along continental margins: Some causes and consequences. *Tectonophysics*, 457(3-4), 197-208.

Sayão, E., França, G. S., Holanda, M., & Gonçalves, A. (2020). Spatial database and website for reservoir-triggered seismicity in Brazil. *Natural Hazards and Earth System Sciences*, 20(7), 2001-2019.

Schaff, D. P., & Waldhauser, F. (2005). Waveform cross-correlation-based differential travel-time measurements at the Northern California Seismic Network. *Bulletin of the Seismological Society of America*, 95(6), 2446-2461.

Simpson, D. W. (1986). Triggered earthquakes. *Annual Review of Earth and Planetary Sciences*, 14(1), 21-42.

Snoke, J. A., Lee, W. H. K., Kanamori, H., Jennings, P. C., & Kisslinger, C. (2003). FOCMEC: Focal mechanism determinations. *International handbook of earthquake and engineering seismology*, 85, 1629-1630.

Snoke, J. A. (1984). A program for focal mechanism determination by combined use of polarity and SV-P amplitude ratio data. *Earthquake notes*, 55, 15.

Stamps, D. S., Flesch, L. M., Calais, E., & Ghosh, A. (2014). Current kinematics and dynamics of Africa and the East African Rift System. *Journal of Geophysical Research: Solid Earth*, 119(6), 5161-5186.

Talwani, P. (1997). On the nature of reservoir-induced seismicity. *Pure and applied Geophysics*, 150, 473-492.

Wilson, M. P., Foulger, G. R., Gluyas, J. G., Davies, R. J., & Julian, B. R. (2017). HiQuake: The human-induced earthquake database. *Seismological Research Letters*, 88(6), 1560-1565.

Wu, Q., Chapman, M. C., & Beale, J. N. (2015). The aftershock sequence of the 2011 Mineral, Virginia, earthquake: Temporal and spatial distribution, focal mechanisms, regional stress, and the role of Coulomb stress transfer. *Bulletin of the Seismological Society of America*, 105(5), 2521-2537.

Zoback, M. L. (1992). First-and second-order patterns of stress in the lithosphere: The World Stress Map Project. *Journal of Geophysical Research: Solid Earth*, 97(B8), 11703-11728.